



OPEN

A new multi-analytical procedure for radiocarbon dating of historical mortars

Sara Calandra^{1✉}, Emma Cantisani², Claudia Conti³, Barbara Salvadori², Serena Barone^{4,5}, Lucia Liccioli⁴, Mariaelena Fedi⁴, Teresa Salvatici¹, Andrea Arrighetti⁶, Fabio Fratini² & Carlo Alberto Garzonio¹

The overarching challenge of this research is setting up a procedure to select the most appropriate fraction from complex, heterogeneous materials such as historic mortars in case of radiocarbon dating. At present, in the international community, there is not a unique and fully accepted way of mortar sample preparation to systematically obtain accurate results. With this contribution, we propose a strategy for selecting suitable mortar samples for radiocarbon dating of anthropogenic calcite in binder or lump. A four-step procedure is proposed: (I) good sampling strategies along with architectural and historical surveys; (II) mineralogical, petrographic, and chemical characterization of mortars to evaluate the feasibility of sample dating; (III) a non-destructive multi-analytical characterization of binder-rich portions to avoid geogenic calcite contamination; (IV) carbonate micro-sample preparation and accelerator mass spectrometer (AMS) measurements. The most innovative feature of the overall procedure relies on the fact that, in case of positive validation in step III, exactly the same material is treated and measured in step IV. The paper aims to apply this procedure to the ancient mortar of the Florentine historical building (Trebbio Castle), selecting micro-samples suitable for dating in natural hydraulic mortars. The discussion of the mortar dating results with the historical-archaeological hypotheses provided significant insights into the construction history of the building.

Keywords Historical mortars, Radiocarbon dating, Geogenic and anthropogenic calcites, ATR-FTIR, Micro-Raman, Microsample preparation

Radiocarbon dating is one of the most widely used dating techniques in the field of archaeology and Cultural Heritage¹. This technique is used to typically date organic finds (such as charcoal, wood, bone, or textiles) but also inorganic materials², such as carbonate compounds, i.e., lead white^{3,4}. Mortar is an artificial product which has been prepared and used by humans since ancient times, mainly consisting of a binder, some aggregates and possible additives.

In mortar and plaster samples, plant remains, such as charcoal, vegetal, and straw fragments, are the most dated fraction with radiocarbon method (¹⁴C), as reported in literature⁵⁻⁷. Other approach concerns the dating with Optically Stimulated Luminescence (OSL) of quartz and feldspar aggregates⁸⁻¹⁰.

In addition, among possible applications to inorganic carbon-based materials, the use of ¹⁴C method for dating ancient mortars was proposed as early as in the 1960s, applying the method to the inorganic binder¹¹⁻¹³. In mortars, the inorganic radiocarbon-datable component is calcite, which is formed by the reaction of calcium hydroxide with atmospheric CO₂ during the setting of the material (the so-called anthropogenic calcite). Air-hardening mortars are the most suitable for dating because they set and harden incorporating atmospheric CO₂. However, since mortars are heterogeneous materials, other sources of C, which may contaminate the ¹⁴C concentration, can be present in the mortar samples.

Contaminations can be due to the presence of:

¹Department of Earth Sciences, University of Florence, 50121 Florence, Italy. ²Institute of Heritage Science, National Research Council of Italy, 50019 Sesto Fiorentino (Florence), Italy. ³Institute of Heritage Science, National Research Council of Italy, 20125 Milan, Italy. ⁴National Institute for Nuclear Physics, Unit of Florence, 50019 Sesto Fiorentino (Florence), Italy. ⁵Department of Physics and Astronomy, University of Florence, 50019 Sesto Fiorentino (Florence), Italy. ⁶Department of Historical Science and Cultural Heritage, University of Siena, 53100 Siena, Italy. ✉email: sara.calandra@unifi.it

- unburned carbonate of stone used for the production of lime and carbonate aggregate present in the mixture (geogenic calcite). These two sources make the sample older than expected;
- (re)crystallized secondary calcium carbonates and products of delayed hardening (so-called secondary calcite). Secondary calcite forms after the initial hardening of the mortar, thus, causing an apparent rejuvenation of the sample.

Moreover, the type of binder of the mortar sample may not be quite ideal, as there are historical mortars with not totally air lime binder.

Selection of the datable fraction and elimination of potential contamination is a challenge for the international radiocarbon community^{14–17}. Despite numerous efforts as evidenced by the extensive literature in the field carried out by the scientific community, an analytical workflow for characterization and dating of inorganic fraction of mortars has not been established.

This paper aims at discussing our sample selection procedure for radiocarbon dating of historic mortars, from the preliminary comprehensive characterization of the material to the sample preparation for the ¹⁴C-AMS measurement. Archaeological and historical survey coupling with accurate sampling, and then in-depth mineralogical and chemical characterization of the mortars are the first two steps (Step I and II), respectively. Separation of binder from the aggregate coupled with characterization of the separated carbonate fractions is mandatory (Step III). Proactive identification of the origin of calcite allows for the reduction of the possible contamination risk, thus obtaining accurate ¹⁴C measurement by AMS (Step IV).

As far as Step II is concerned, a multi-analytical characterization procedure of the mortar fragments, i.e. optical and electron microscopy (OM, SEM-EDS), X-ray diffraction on powders (XRPD), thermogravimetric analysis (TGA), infrared spectroscopy (FTIR) was designed.

In Step III, a non-destructive, original approach capable of identifying the origin of calcite (geogenic and anthropogenic calcite) was explored using XRPD, OM-cathodoluminescence (OM-CL), ATR-FTIR, micro-Raman. A new experimental set-up for the collection of CO₂ evolving from the selected calcite was installed, by integrating an acidification reactor into our so-called Lilliput graphitization reactors, which are optimized for microgram-sized samples^{18,19}. The graphitization line is used to obtain graphite samples whose residual ¹⁴C abundance is measured by AMS.

The procedure was validated in architectural contexts, such as the Tuscany historical building (Trebio Castle in Florentine surroundings).

Analytical procedure

Step I: sampling and the issue of chronology questions

Accurate dating of mortar in masonry requires a comprehensive approach involving collaboration between experts in mortar analysis, archaeologists and architects who understand wall stratigraphy^{20,21}. Precise sampling is crucial and begins with well-defined research questions related to chronology, along with documentation and historical research and analysis of the masonry²² (Fig. 1, step I). For example, if the aim is to determine the age of construction, it is important to avoid areas of repair or renovation. However, if the focus is on determining the period in which the building was in use, these repaired or renovated areas may be of greater importance. Mortar between stone blocks is likely to be original if the stone block overlies the mortar; on the other hand, if the mortar protrudes beyond the stone block, this indicates a later intervention. Care should be taken when

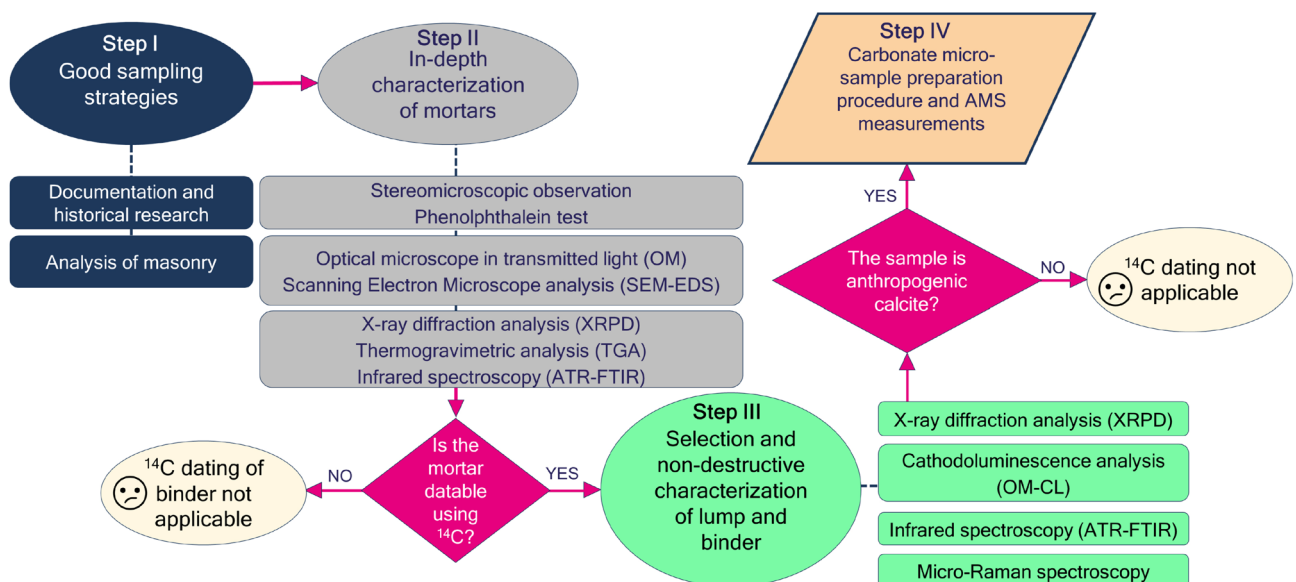


Fig. 1. Graphical representation of the new multi-analytical procedure for radiocarbon dating of historical mortars.

selecting samples from the ground, i.e. from collapsed ruins, as these may have been transported or weathered, thus being their association with the event to be dated not accurate.

Mismatches in the dating results can arise due to different factors, such as mortar constituents (the type of binder and aggregate) or environmental factors (the state of preservation, which may be due to e.g. recrystallization and delayed hardening).

For instance, bedding mortars or core mortars are generally less altered over time than plaster and are less exposed to the external environmental parameters²³.

To minimize secondary carbon sources, sampling sites should be carefully selected, favoring areas that are less exposed to weathering over exterior surfaces^{20,21}. Analyzing samples from greater depths and intermediate heights helps to mitigate the influence of ambient water, which can introduce younger samples through rainfall or surface water or obvious aging effects from dissolved geological carbonates in groundwater and soil moisture.

As the slaked lime ($\text{Ca}(\text{OH})_2$) absorbs CO_2 from the atmosphere, the setting and hardening process starts from the surface and progresses inwards. Delayed hardening in the inner parts of thick walls can lead to inaccuracies in dating results²⁴. Optimal samples should be taken at a depth close to the wall surface, deep enough to avoid problems with the surface, but not too deep to have problems with delayed hardening. If carbonate aggregates are present, careful sampling is essential to limit dispersion.

In summary, careful sampling and consideration of various factors are crucial for successful ^{14}C dating results in mortar. These considerations and methods contribute to the robustness and reliability of mortar dating in archaeological investigations.

The evaluation of the degree of carbonation of the mortar with the phenolphthalein test is the first mandatory characterization step. Phenolphthalein indicates the presence of calcium hydroxide in the mortar. A sample that is not fully carbonated must be excluded for ^{14}C dating. The test can be carried out in situ on the masonry or in the laboratory on a sample.

Step II: analytical procedure to characterize mortars for dating

To characterize mortars and select those materials that can be suitable for dating purposes, it is essential to determine the composition of all the constituents of the mixture, their relative amounts (binder/aggregate ratio—B/A), the nature of binder and aggregates, the constituents within the binder, as well as the degree of carbonation. In fact, the information we can get from different analytical techniques can give us hints about the manufacturing process of the materials. In particular, it can suggest us whether the basic conditions for applying radiocarbon dating are respected and can support us to choose the best approach to select the most appropriate fraction to be dated. For example, the aforementioned B/A ratio allows us to understand how much material we have to sample to get enough mass at the end of the selection procedure.

For a comprehensive characterization, several investigations must be performed, each useful in reconstructing the overall picture and providing key information to select or exclude material for dating (Fig. 1, step II). The complementarity of multiple investigations is crucial for an accurate and full understanding of the material. Indeed, the investigations make it possible to determine the relative chronology of different construction phases within a building or site^{25,26}. Here following the summarized description of the analytical techniques proposed for characterization.

OM

Thin-section observation of mortar under an OM in transmitted light provides essential insights into the nature of binder, aggregate and lumps^{19,27}.

For the binder, OM provides information on the texture (micritic, microsparitic, sparitic), the mineralogical composition, the birefringence colors, the structure and the interactions with the aggregate. Moreover, OM allows us to classify the binder as: air lime, natural hydraulic lime, air lime with addition of pozzolanic materials (i.e. *cocciopesto*, volcanic ash and clay minerals) and modern hydraulic binder^{28,29}.

The description of the aggregate is crucial for the evaluation of contamination sources, taking into account mineralogical composition, particle size distribution, amount of binder with respect to aggregate (B/A) ratio, macroporosity and alteration products.

Petrography is also beneficial for the identification of lumps and organic fragments in the mortar. OM observation make it possible to recognize the type of lumps and distinguish between residues of stones used to make binders and binder residues.

The observation of lumps with OM allows us to recognize their types and origins, achieving information on the rock used to produce lime as well as suggestions on production technologies²⁷.

Petrographic observation contributes to assess the uniformity of the binder and to identify zones of different crystallinity due to partial recrystallization by circulating water. Sources of contamination, such as recrystallization of calcite and carbonate aggregates, can lead to exclude samples from ^{14}C dating²¹.

Modern binders should be eliminated from dating, since the dating principle is not applicable to these types of binders. Particular attention should be paid to magnesium binders³⁰. The ^{14}C dating outcomes may be affected by the presence of much younger ^{14}C , due to the properties of minerals produced upon carbonation (such as magnesite and nesquehonite).

XRPD

XRPD analysis of bulk samples includes the mineralogical composition of both the binder and the aggregate, which can be integrated with the identified phases in thin sections. Single lumps and binder-rich portions can be also analyzed. All these data yield crucial information, revealing whether the mortar is non-carbonated (portlandite), if the sample contains magnesium lime (brucite, hydromagnesite, magnesite), or if the binder

exhibits hydraulic properties³¹ (tobermorite, hydrogarnet), or if secondary reactions occurred which lead to the formation of new phases (gypsum, hydrotalcite, hydrocalumite). The presence of these latter two phases in mortar binders strongly influences the radiocarbon dating of lime mortars, because of their high (CO₃)²⁻ anion capture capability^{32,33}. The presence of gypsum indicates that the binder has altered, suggesting an open system and therefore a context subject to contamination from the external environment³⁴.

SEM-EDS

Observations under the optical microscope can be further enhanced and supplemented by SEM-EDS which combines microscopy and X-ray spectroscopy to obtain detailed information on the morphology and elemental composition of mortar constituents. Semi-quantitative elemental analysis is useful for: (1) estimating the provenance of raw material through the analysis of residues of stones used for lime production; (2) obtaining information on the hydraulic index (HI)³⁵ and the overall composition of the binder, including the possible presence of Ca and Mg based binder, and of silico-aluminates ferriiferous phases; (3) evaluating changes in elemental composition within reaction rims areas; (4) characterizing lumps, especially if they have a heterogeneous texture; (5) achieving micro-chemical information about the aggregate and providing hypothesis on its provenance.

TGA

TGA is used in the analysis of historical mortars for evaluating hydraulic behavior; it involves subjecting a sample to controlled temperature changes while measuring its mass as a function of temperature. TGA serves for characterization of binder materials (air binder, hydraulic binder, gypsum, etc.)^{36,37}. Moreover, the TGA results can be integrated with the HI value calculated from punctual micro-chemical analyses carried out with SEM-EDS³⁸.

Step III: Selection and characterization of the powder for the screening of CaCO₃ origin

Upon assessing that the sample exhibits datable characteristics, as a consequence of all the analyses performed in Step II, the following process involves the selection and further characterization of the carbonate fraction. The binder calcite has the same chemical composition as burned carbonate rocks or carbonate aggregates, but different textural, isotopic signatures and mechanical properties.

A mechanical separation of binder-rich bulk and lump was performed, starting from a selection under stereomicroscope. For bulk samples, a portion enriched with binder and lumps is separated, then sieved to 63 μm and lightly crushed.

Our approach aims at finding non-destructive techniques able to determine the origin of the calcite in the powder samples selected for dating (Fig. 1, step III). Non-destructive techniques allow the preservation of the sample mass so that the same sample can be subjected to several analytical procedures and treated for ¹⁴C analysis (Fig. 1, step IV).

The different origin of carbonates (geogenic and anthropogenic) can be detected by the different distortions in the lattice structure within small crystallites. In principle, different types of calcite interact with electromagnetic radiation in a way that depends on the atomic arrangement. FTIR and Raman spectroscopies can be used to identify short-range order at the molecular level. In addition, CL analysis, which is conventionally used to assess the origin of calcite, in our approach is combined with ATR-FTIR and micro-Raman.

The most important advantage in this non-destructive approach is that the exactly same powder is analyzed in OM-CL, ATR-FTIR and micro-Raman; and if the sample is mainly constituted by anthropogenic calcite, it is used for step IV.

OM-CL

CL is a petrographic technique which represents an additional way of examining thin sections or powder samples of carbonate specimens³⁹. The phenomenon of CL of mortars has been discussed since 1997 and has been used in numerous studies to evaluate the origin of carbonates^{13,40,41}. Different densities and distribution of atomic defects in the calcite crystal structure serve as markers to identify the origin of calcite. Considering this principle, geogenic calcite and anthropogenic calcite may have different luminescence intensities due to the different formation process.

The phenomenon can be easily observed with petrographic microscopes equipped for CL analysis (OM-CL), this instrumentation is relatively inexpensive and easy to use. For the non-destructive analysis of powders, we used OM-CL. The disadvantage of this technique lies in the resulting color hues, especially when multiple emissions of the same powder result in a composite hue. Typically, a qualitative analysis was performed, just attributing “hues” to the different observed colors (see for example tile red, dull purple, brown, dark brown, grey, dull grey and black). In such a framework, interpretation of data could be influenced by the operator him/herself^{20,42,43}. This problem can be solved by combining several analytical techniques to obtain a validated and unambiguous result.

FTIR

In the context of mortar dating, spectroscopy has already been used to distinguish the origins of calcite. As demonstrated in previous studies^{44–46} conventional Fourier transform infrared spectroscopy in transmission mode with KBr pellets can be employed for rapid sample analysis, using the heights of ν_2 and ν_4 bands.

In order to use non-destructive analysis and preserve the sample for further analysis and dating, ATR-FTIR was tested on samples with known composition and origin to establish whether this mode could lead to the same results as the FTIR technique with KBr pellet⁴⁷.

Since it has been shown that differences in grinding degree affect peak widths and relative heights of carbonate archaeological materials^{34,48}, samples with same preparation procedures were analyzed to replicate the typical pre-treatment that might be carried out on unknown samples for dating purposes.

The distinct trend lines highlight the systematic differences in ν_2 versus ν_4 peak heights in ATR-FTIR mode for calcites formed through various processes. Two trend lines were created (geogenic and anthropogenic calcites), which can help to determine the origins of unknown samples, offering preliminary insights into their formation. The ability to discern calcite origins through the ATR technique is particularly advantageous in the field of mortar dating, as powdered samples can be collected and reused for dating if they contain anthropogenic calcite.

Micro-Raman

Micro-Raman spectroscopy is a valuable tool for the characterization of mortars, enabling high lateral resolution analysis of the mineral phases of aggregates and binder components^{49,50}. So far, some studies have demonstrated that micro-Raman spectroscopy can be successfully used to estimate the content of cations (Mg^{2+} , Fe^{2+} and Mn^{2+}) in carbonates, as the vibrational frequencies of the translational (T) and librational (L) modes of carbonates are significantly related to their cation composition^{51,52}. Raman spectroscopy has been used to investigate variations in atomic bonding in biogenic calcite crystals and to distinguish the degree of crystallinity of calcium carbonate in biological materials by assessing the frequencies and width of the ν_1 and ν_4 bands⁵³. Raman analysis of CaCO_3 polymorphs in⁵⁴ found that the amorphous calcium carbonate exhibits a broad peak in the lattice mode region (below 400 cm^{-1}) and that the most prominent band associated with the carbonate ion at around 1085 cm^{-1} , which appears as broader and significantly less intense than usual, slightly shifts towards lower wavenumbers.

We carried out a study to determine the origin of calcite using micro-Raman spectroscopy. The potential to distinguish between geogenic and anthropogenic calcite using micro-Raman spectroscopy was established for the first time by the authors⁵⁵.

Raman spectroscopy and statistical methods have shown that the anthropogenic calcite samples exhibit a broadening of the L, ν_1 and ν_4 bands (calculated from FWHMs) compared to geogenic calcite samples.

Structural disorder within the calcite crystals or the presence of low crystalline order is reflected in relatively broad FWHM values and wavenumber shifts. The wider and shifted toward lower wavenumber is the spectral band, the lower the crystallinity within the mineral.

The influencing parameters (including band position, band intensity, the area covered by the bands and the FWHM values of L, ν_4 and ν_1) for distinguishing the origins of calcite were successfully identified and they can be used to determine the origin of calcite in unknown samples intended for dating.

The potential of micro-Raman on distinguishing different calcite domains was also confirmed by Toffolo et al.⁵⁶. In this paper, the micro-Raman analyses were performed on petrographic thin sections in archaeological lime samples.

Step IV: carbonate micro-sample preparation and AMS measurements

The limited sample material due to the high possible level of heterogeneity of the mortars, the sample loss during the characterization step and the highly selective pre-treatment process, motivates us to use the micro-sample ^{14}C preparation.

In this framework, the so-called Lilliput graphitization line at the LABEC laboratory in Florence, one of the laboratories of CHNet, the INFN network for Cultural Heritage, was integrated with a reaction chamber designed for the extraction of CO_2 from carbonates (Fig. 1, step IV). The Lilliput line is particularly useful in the case of mortar treatment, because it allows managing samples as small as only $50\text{ }\mu\text{g}$ of carbon, well below the limit of the “traditional” larger samples of about $700\text{ }\mu\text{g}$ ^{18,57}. Such small processed masses provided the possibility to investigate the feasibility of dating even individual lumps of binder in mortar samples.

Typical processing masses for mortar samples are:—approx. 2.5 mg in the case of lump; —approx. 5 mg in the case of bulk mortar.

Acid dissolution and Lilliput graphitization reactors

The extraction of C from the selected inorganic fraction of the mortar is carried out by acid dissolution. The carbonate sample, mechanically separated and previously characterized with non-destructive techniques, is treated with H_3PO_4 in the acidification line.

For bulk samples, 2 evolving CO_2 fractions are usually collected per sample: the first in a few seconds (0–10/30 s) and the second thereafter (10/30–60 s). The selected shortened reaction time is intended to avoid the risk of geological contamination, at least in the first fraction, as contaminants may still be present despite mechanical separation. In the case of lump samples, a fraction from the first few seconds of the reaction is collected without the risk of contaminants reacting with the acid.

The CO_2 extracted from the acidification line is then cryogenically transferred into the graphitization chamber using liquid nitrogen. The amount of CO_2 collected is monitored by pressure measurements. Typically, about 100 mbar of CO_2 is collected for each sample; this pressure basically corresponds to about $50\text{ }\mu\text{g}$ of graphite at the end of the reaction given the inner volume of the Lilliput reaction chambers. The graphitization reaction occurs on small copper inserts previously prepared with Fe catalyser pressed on them and is triggered at $600\text{ }^\circ\text{C}$ in presence of H_2 excess; the reaction produces water, which is trapped within the cold finger. After the graphitization process, the copper inserts with the graphite deposited on them are mounted in specially modified aluminum holders that fit into the ion source of the accelerator to measure the radiocarbon concentration.

Results and discussion

Application of the procedure on historical building: Trebbio Castle

Step I

The analytical procedure for dating was applied to mortar samples from the walls of the tower of the Trebbio Castle, one of the most important and significant examples of aristocratic villas owned by the Medici in the area around Florence (Mugello)⁵⁸ (Fig. 2).

The building was investigated through the building archaeological approach, which identifies the stratigraphic units of the building, and then associated with written or other sources, allowing the formulation of hypotheses about the construction phases of the masonry⁵⁹.

Based on this methodology, four main construction phases from the thirteenth century to the first decades of the seventeenth century, were identified:

- Phase 1 (before 14th cent.): the presence of a square tower is documented. The tower was partially rebuilt and its original structure is only visible in the lower part.
- Phase 2 (14th cent.): addition of storeys to the pre-existing tower with improved masonry and crenellated walls, characterized by different building construction techniques than the previous phase.
- Phase 3 (1420–1433): addition of new storeys to the tower and complete renovation of the upper structure, including corbels and wider walkways, attributed to Michelozzo (as reported written source in⁶⁰).
- Phase 4 (post 1433): modern and contemporary restorations, including mortar sealing, reconstruction and rectification of structural problems to restore a late medieval appearance. Some restoration works were performed following the numerous historical earthquakes that affected the Mugello area⁵⁸.

The chronology of the building phases is the result of a combination of stratigraphic studies, written sources and the chronotypical abacus of Mugello masonries⁵⁸.

The archaeological reading of the masonry and the resulting hypotheses about the construction phases formed the basis for the selection of the mortar sampling points. A total of 27 bedding mortar and plaster samples were collected using a hammer and chisel (Supplementary Table 1).

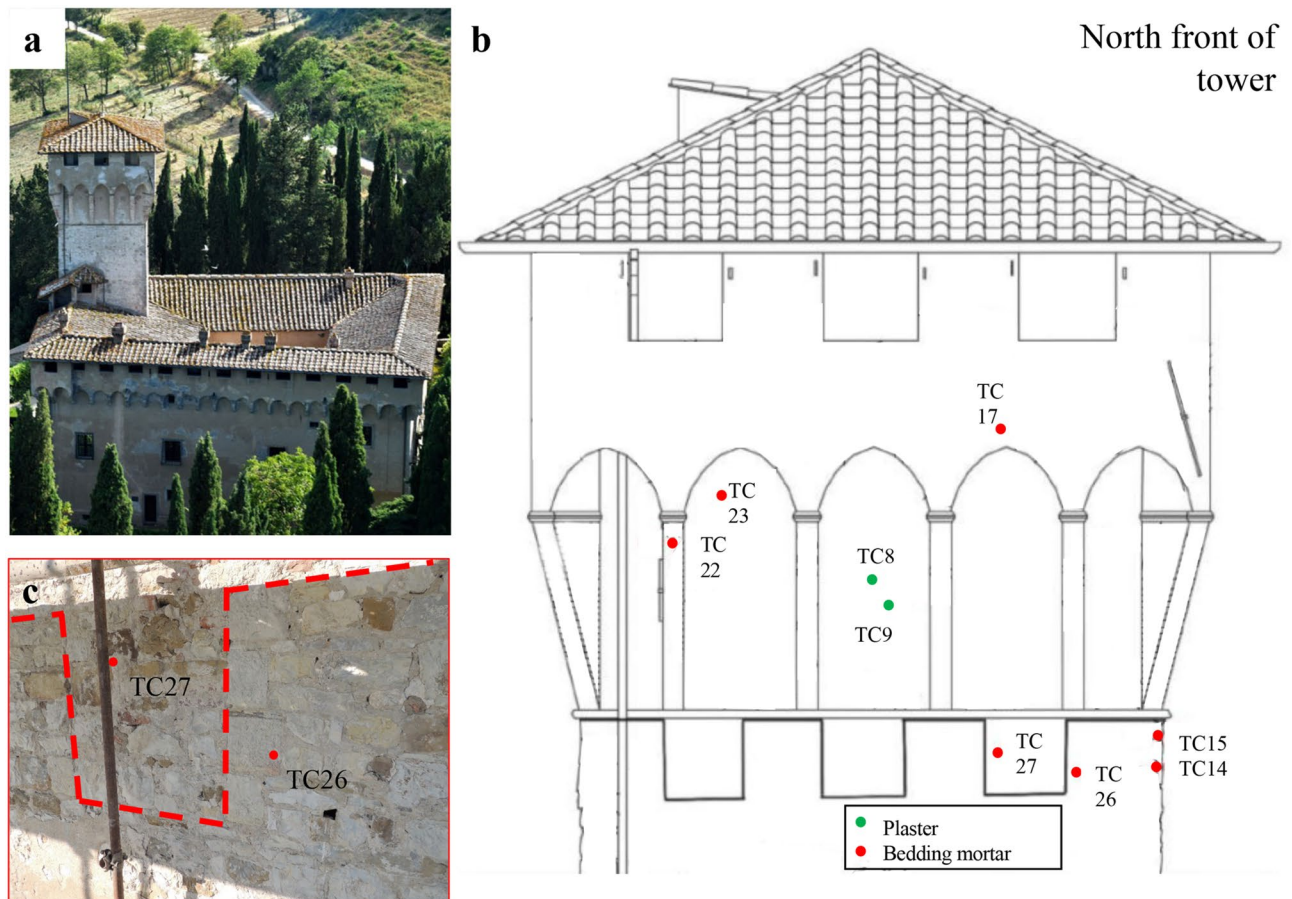


Fig. 2. Trebbio Castle: building (a); sampling on the North side, perspective drawing (by Teresa Salvatici and Sara Calandra) (b), and masonry (c).

Step II

The comprehensive minero-petrographic characterization was performed on all mortar samples (Supplementary Table 2).

Mineralogical composition analysis of bulk mortars by XRPD revealed the presence of calcite, quartz, feldspar (plagioclase and k-feldspar), lizardite and micas. Calcite can be referred to the binder, lime lumps or fragments of aggregate; quartz, feldspars, lizardite and micas can be related to the aggregate. Gypsum was recorded only in TC19 and 24, probably due to the sulphation phenomena of the binder³⁴, Supplementary Fig. 1.

From the petrographic observation, these mortars are made of natural hydraulic binder, obtained by firing of marly limestone (Alberese limestone, Monte Morello Formation), diffusely employed in Florentine area⁶¹. The aggregate exhibits a heterogeneous composition, utilizing sandy sediments from local watercourses. Finer sands (< 400 µm) predominantly consist of single crystals of quartz, feldspars, spathic calcite, while coarser fractions contain fragments of arenaceous rocks, serpentinites, and Alberese limestone. Rare fragments of cocciopesto were also found.

Since the raw materials used are the same and the production technologies are similar, no minero-petrographic criteria were identified to differentiate samples belonging to different construction stages. Within the same construction stages, different characteristics are found in the mix-design (i.e., B/A, grain size distribution).

For radiocarbon application we focused on the binder aspect, aggregate composition and the presence of lump. So, the binder in the plaster samples (TC1-11, Supplementary Fig. 2a, b) has undergone some chemical alteration due to the dissolution and slow recrystallization of calcite by the circulating moisture in the masonry. This process can develop in specific areas of the samples, e.g. in pores and along fractures (referred to as secondary calcite) or change the entire texture of the binder (referred to as partially binder recrystallization). This prevented us from selecting these samples for dating, causing an apparent rejuvenation of the sample⁶².

As for the bedding mortars, the binder is better preserved. Care in the preparation of the mixtures is evident, considering careful selection of aggregates and a consistently high binder content. However, even these samples exhibit characteristics that allow the selection of only certain samples for dating: samples superficially collected, those with non-homogeneous carbonation processes (heterogeneous texture ranges from microsparitic to sparitic in TC12, 13, 14, 15, 16, 18, 22, 24, 25, Supplementary Fig. 2c, d), or binder recrystallization (as in TC12, 13, 14, 15, 16, 17, 18, 19, 21, 22, 24, 25), those showing gypsum in XRPD (as in TC19, 24), and those with almost exclusively carbonate aggregate (TC20, 23; Supplementary Fig. 2e) have been excluded. Heterogeneous texture can be due to delayed carbonation processes or binder dissolution-recrystallization⁶³, in fact, in most samples the two features are combined.

Within bedding mortars, we focused on two samples that could provide key insights into the historical attribution of construction phases and with mineralogical-petrographic characteristics which are more suitable for dating. These samples come from the crenellated masonry, TC26, and the infill masonry, TC27 (see in Fig. 2c). The samples show complete carbonation through phenolphthalein test. On initial macroscopic examination, sample TC26 appears to have a compact mortar with few fractures and a hazel coloration. Millimetre-sized lumps of varying coloration, from white to yellowish, are visible. The mortar sample TC27 is compact and has a hazel color. Millimetre-sized lumps of yellowish to white hues can also be observed.

The main mineralogical and petrographic characteristics of these two samples are listed in Table 1.

Petrographic observations of TC26 and TC27 reveal the presence of a binder with homogeneous structure and micritic texture with small dark inclusions. Lumps are present, referring to both unmixed binder and unburned limestone.

The aggregate exhibits a heterogeneous composition and bimodal grain size distribution, consisting of abundant carbonate rock fragments (limestone and calcarenites), sandstone, serpentinite and crystal of quartz,

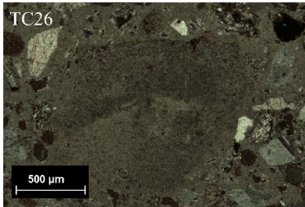
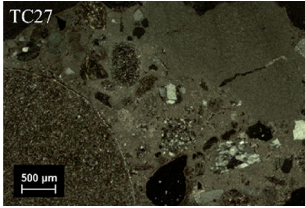
ID sample (OM)	Binder	Aggregate	B/A	Macroporosity	XRPD
	Natural hydraulic lime with homogeneous structure and micritic texture with small dark inclusions Presence of lumps (unmixed lime, unburned rock)	Composition: fragments of sandstone and micritic limestone, single crystals of quartz and plagioclase, secondarily sparitic calcite and rare serpentinite fragments Bimodal grain size distribution Grain size: 200–300 µm, 700–800 µm. Shape: subangular-subrounded	1/3	Low amount due to shrinkage fractures	Calcite, quartz, plagioclase, lizardite, micas, clay minerals
	Natural hydraulic lime with homogeneous structure and micritic texture with small dark inclusions Numerous lumps (unmixed lime, unburned rock)	Composition: fragments of sandstone and micritic limestone, single crystals of quartz and plagioclase, secondarily sparitic calcite and rare serpentinite fragments Bimodal grain size distribution Grain size: 200–300 µm, 0.7–1 mm. Shape: subangular	1/2	Low amount due to shrinkage fractures	Calcite, quartz, plagioclase, lizardite, micas

Table 1. Petrographic and mineralogical characteristics of TC mortar samples.

feldspars, and calcite (Supplementary Fig. 3). TC26 and TC27 differ in: the B/A, 1/3 and 1/2, respectively, and for the coarser aggregate grain size in sample TC27 (0.7–1 mm).

SEM–EDS analyses on the binder showed significant variability in SiO₂ and CaO content, along with the presence of different types of lumps, confirming the use of Alberese limestone. A comprehensive study of lumps, combining OM, OM-CL, and SEM–EDS analyses in the same area, revealed that also the texture of lumps is heterogeneous (Fig. 3). They exhibit a similar texture to the binder in OM, appearing brick-red in CL, and SEM analysis indicates a CaO and SiO₂ + Al₂O₃ + Fe₂O₃ composition comparable to that of the binder. SEM–EDS analysis of the thin sections indicates that only small amounts of Mg are present (less than 1.8%). To gain further insight into the binder composition, SEM–EDS microanalyses were carried out on polished thin sections of both binder and lime lumps. The micro-chemical composition of lime lumps and binder is reported in Table 3. In addition, the hydraulicity index (HI) was calculated using Boynton's formula³⁵ (Table 2). TC26 exhibits an HI of 0.16 ± 0.05, TC27 shows an HI of 0.20 ± 0.08, classifying as weakly hydraulic.

HI results are compared with TGA analyses performed on 3 portions of binder-rich mortar per sample.

The hydraulic water (%) originating from the hydraulic components varies between 7.02% and 8.89%, while the CO₂ decomposition from air lime binder is between 27.0% and 31.9%. The results of SEM–EDS are in agreement with those of TGA and show that the mortars have slightly hydraulic behavior (Supplementary Fig. 4).

Step III

Being carbonate aggregates abundant, to avoid possible contamination, we decided to focus on lumps for dating. Four lumps were selected for TC26 samples (labelled as TC26L1, L2, L3, and L4), and four for samples TC27 (labelled as TC27L1, L2, L3 and L4) (Fig. 4a).

XRPD analyses were conducted on the powdered lump samples after sieving to determine mineralogical composition (Table 3); OM-CL, ATR-FTIR and micro-Raman analyses (Fig. 4b–d) were performed to assess the origin of the calcite.

XRPD analysis on lumps showed that the primary component is calcite, as expected.

TC26L1, TC26L2, TC26L4, TC27L1 and TC27L4 exhibit red-brown luminescence, which is consistent with their position on the anthropogenic calcite trend in ATR-FTIR, classifying them as pyrogenic carbonate.

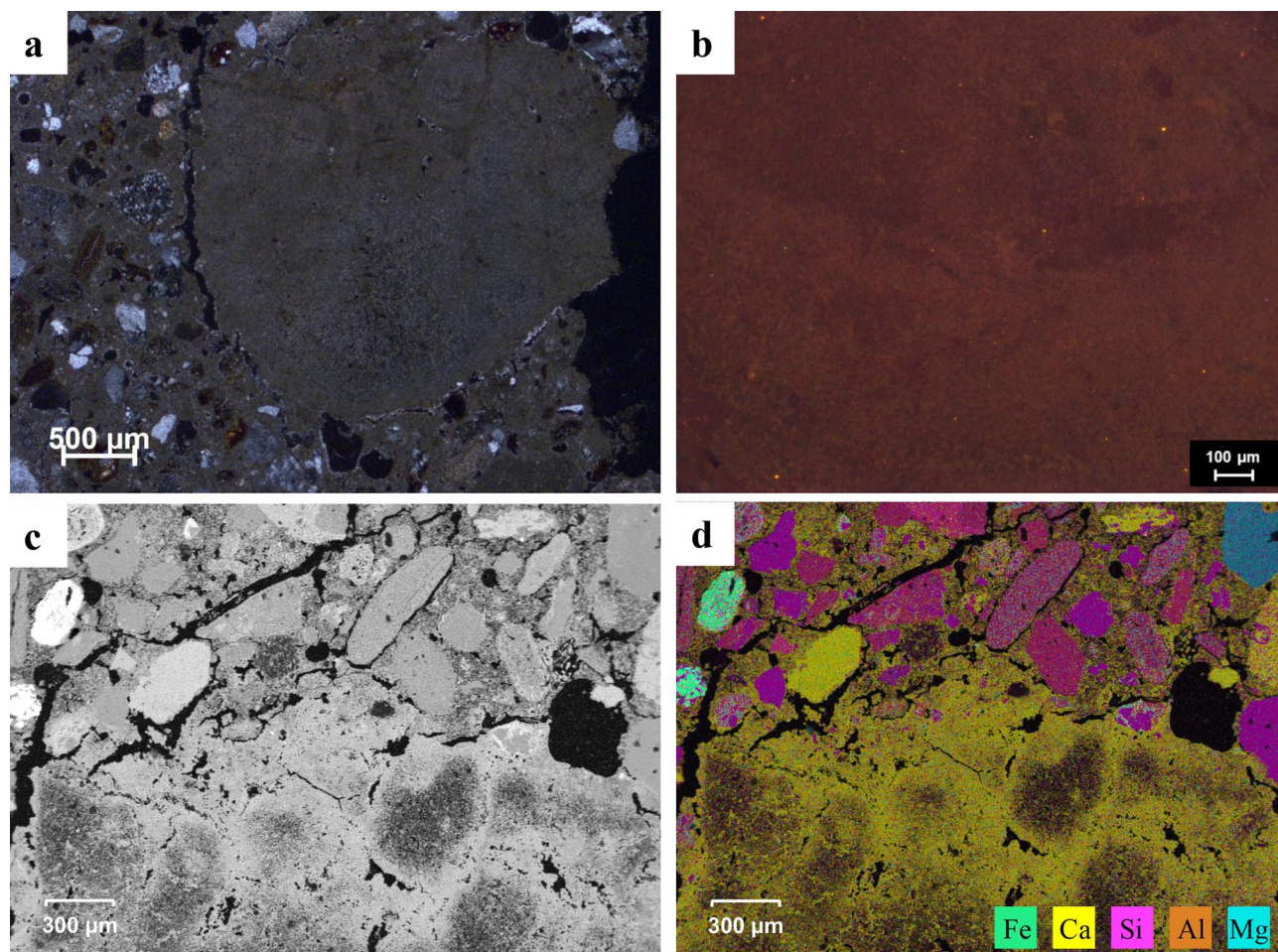


Fig. 3. OM (a), OM-CL (b), SEM–EDS (c, d) analyses on lime lump. In (c), BS image of a detail of the lump. In (d), SEM–EDS map layered on the previous area.

TC26	Lime lump	Lime lump	Lime lump	Binder	Binder		
SiO ₂ + Al ₂ O ₃ + Fe ₂ O ₃	10.0	11.1	17.5	17.6	12.6		
CaO + (MgO)	90.1	89.0	82.5	82.4	87.4		
HI	0.1	0.1	0.2	0.2	0.1		
TC27	Lime lump	Lime lump	Binder	Binder	Binder	Binder	Binder
SiO ₂ + Al ₂ O ₃ + Fe ₂ O ₃	17.6	11.9	21.8	19.5	10.7	22.8	8.7
CaO + (MgO)	82.1	88.1	78.2	80.5	89.3	77.2	91.3
HI	0.2	0.1	0.3	0.2	0.1	0.3	0.1

Table 2. Semi-quantitative SEM–EDS micro-chemical analyses (wt%) of binder and lime lumps for the HI calculation.

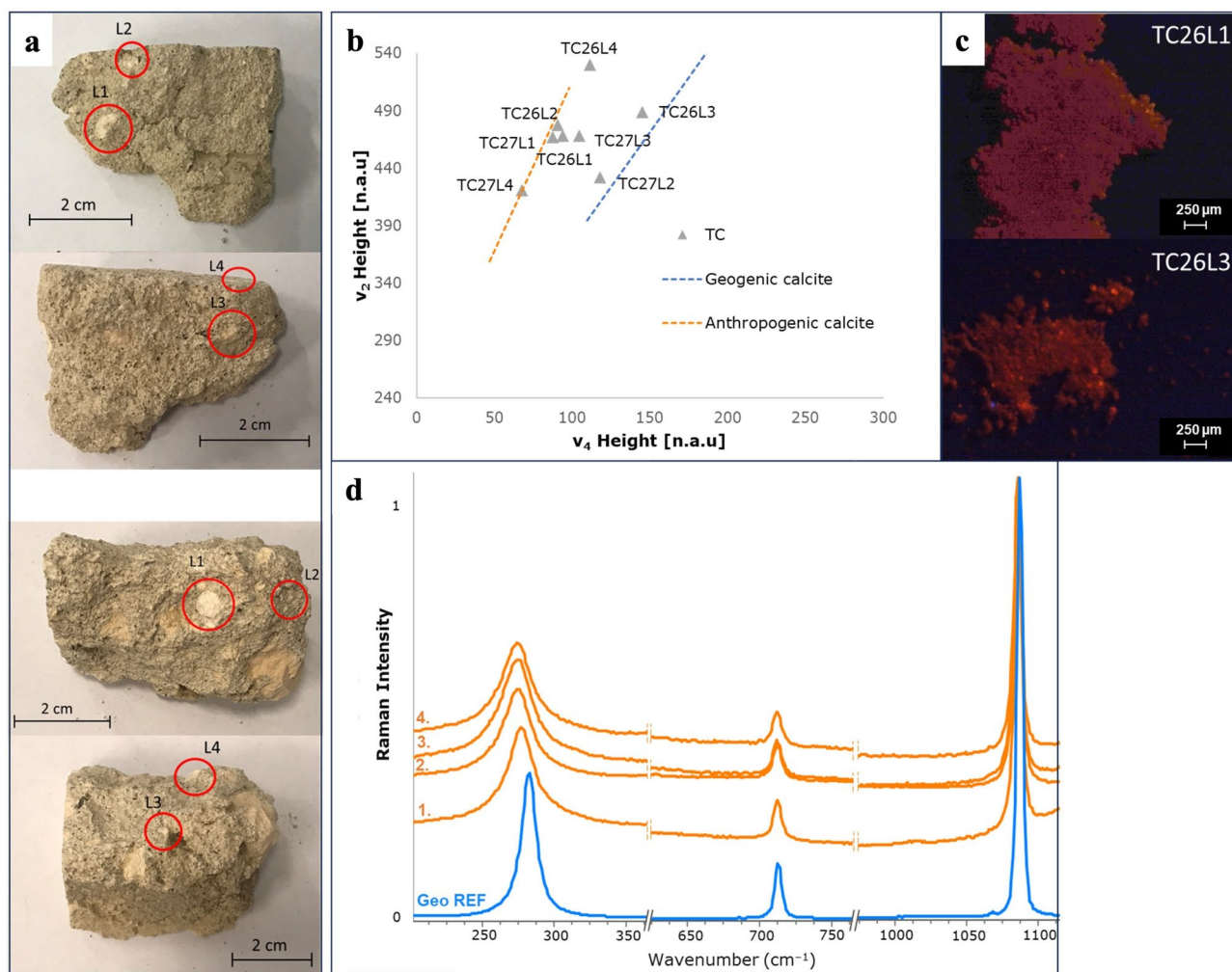


Fig. 4. Results of non-destructive techniques on powders (**b–d**) and lump selection points (**a**). Plot of v_2 and v_4 with typical trend lines of geogenic and anthropogenic calcites obtained by ATR-FTIR and TC lump samples (**b**); OM-CL photomicrographs of lump powders: an anthropogenic sample (TC26L1) and a geogenic sample (TC26L3) (**c**); comparison among individual Raman spectra of carbonate samples: geogenic calcite (in blue, a reference sample) and anthropogenic calcite of TC samples (1: TC26L1; 2: TC26L2; 3: TC26L4; 4: TC27L1) (**d**).

However, TC26L3, TC27L2, and TC27L3 exhibit orange CL and geogenic trends in ATR-FTIR, confirming that these lumps consist of geogenic calcite. ATR-FTIR detected a broad band centered at 1080 cm^{-1} , attributable to $\nu_{\text{as}}(\text{Si-O-Si})$ and ascribed to amorphous silicates⁶⁴, likely originating from the calcination of stone rich in silicate components (e.g., clay minerals) (Supplementary Fig. 4).

Micro-Raman analyses, conducted on TC26L1, TC26L2, TC26L4, TC27L1, TC27L4, show a Raman shift of L and ν_1 bands toward lower wavenumber, along with their higher FWHM values, which is also observed for

ID sample	XRPD	L wavenumber	L FWHM	ν_4 wavenumber	ν_4 FWHM	ν_1 wavenumber	ν_1 FWHM
TC26L1	Cal (xxx), qz (x)	275.0	24.3	712.1	7.2	1085.4	5.9
TC26L2	Cal (xxx), qz (*)	277.4	20.2	712.4	6.5	1085.8	5.3
TC26L4	Cal (xxx), qz (x)	277.2	19.3	712.4	6.6	1085.8	5.4
TC27L1	Cal (xxx), qz (*)	277.8	18.1	712.5	6.3	1086.0	5.2
TC27L4	Cal (xxx), gp (*)	273.8	26.6	712.2	7.5	1085.4	6.4

Table 3. XRPD and Raman results of calcite mortar powders. The average of the wavenumbers, FWHMs of L , ν_1 , ν_4 from 10 Raman measures performed for each sample. Cal, calcite; qz, quartz; gp, gypsum; xxx, very abundant; xx, abundant; x, present; *, traces; -, below detection limit.

the ν_4 band (Table 3). The micro-Raman results definitively confirm the data collected by other techniques. The observed values are typical of anthropogenic calcite.

Step IV

Based on the result of the characterization process discussed in the previous sections, lumps TC26L1, TC26L2, TC26L4 and TC27L1 were chosen to be suitable for dating. The reaction times, along with the masses of the graphitized samples, are listed in Table 4. The reaction time of 30 s was chosen since, having assessed the anthropogenic origin of the calcite, the risk of contaminants reacting with the acid and the sample mass were low. The AMS results are reported in Table 4.

When samples belonging to the same fragment or construction phase have consistent radiocarbon concentration between each other, a weighted average can be calculated to obtain a more precise result. Indeed, the lumps TC26L1, TC26L2, and TC26L4 from the same mortar portion exhibit consistent radiocarbon concentrations. The results of the weighted average of the three radiocarbon concentrations and the corresponding conventional radiocarbon age are also reported in Table 4.

The calibrated age for samples TC26L1 + TC26L2 + TC26L4 results from the measured conventional radiocarbon age (Fig. 5).

Although the calibrated age of the TC26 lump samples spans two of the phases identified in the archaeological analysis of the tower (phases 2 and 3), the characteristics of the masonry where the sample was taken suggest an interpretation of the ^{14}C results as more likely within the middle of the fourteenth century (phase 2).

The dating results for sample TC27L1 are presented in Table 4. Given the conventional radiocarbon age measured (Fig. 5), sample TC27L1 is considered modern. A discrepancy can be observed between the assumed

ID samples	Mass (mg)	Reaction time (s)	^{14}C concentration (pMC)	T_{rc} (yrs BP)	Calibrated age (95% probability)
TC26L1	4.08	0–30	93.8 ± 1.7	528 ± 66	1296–1472
TC26L2	2.62	0–30	93.4 ± 1.1		
TC26L4	2.34	0–30	93.9 ± 1.4		
TC27L1	2.10	0–30	98.4 ± 1.0	130 ± 82	1657–...

Table 4. Acid dissolution information (lump mass, reaction time chosen for the acid dissolution) and AMS results of TC samples.

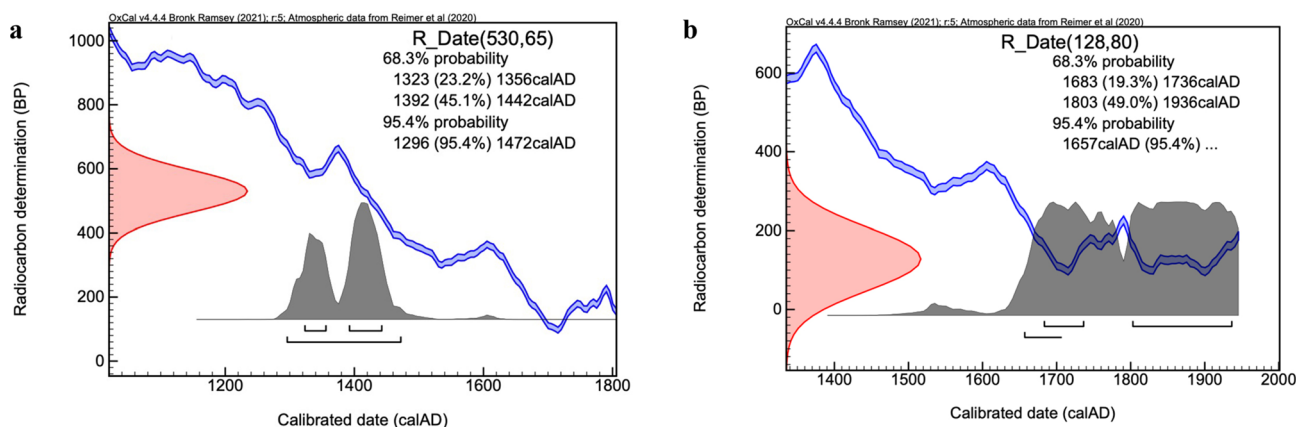


Fig. 5. Calibrated age of the TC samples: TC26L1 + TC26L2 + TC26L4 (a); TC27L1 (b).

chronology and the measurement of the radiocarbon concentration. Based on the historical-archaeological hypothesis, it is assumed that the masonry dates from the middle of the fifteenth century (phase 3).

However, this discrepancy could be related to the extensive joint sealing of the upper part of the tower. The combination of the calibrated age and the historical information; allow us to formulate a specific interpretative hypothesis and attribute this operation to the restoration season following the seismic events that affected the Mugello area between the mid-15th and mid-seventeenth centuries⁵⁸. After this intense and destructive earthquake period, intensive restoration and reconstruction activities were carried out on all the Medici properties in the area (e.g. Cafaggiolo, the Fortezza di San Martino, the town of Scarperia). Sample TC27, being associable to the modern phase, could have intercepted one of these activities.

The comparison between the radiocarbon dating and the archaeological results offered two new interpretations. On the one hand, the ¹⁴C dating for sample TC26 yielded a range of dates that included the fourteenth and fifteenth centuries, while the chronotypology of the masonry of Mugello allows us to shift the focus to the first one. TC27, on the other hand, it was the ¹⁴C dating that provided new interpretative approaches to the historical-archaeological data and made it possible to identify specific restoration interventions carried out in the modern period on a masonry that in the written source dates to the early fifteenth century⁶⁰.

Conclusion

The proposed multistep procedure is demonstrated to be a successful approach for selecting a suitable mortar sample for radiocarbon dating. Multi-analytical approach (OM, SEM–EDS, XRPD, TGA) has been proven to permit the selection of the most suitable mortar to be dated. Non-destructive analyses (XRPD, OM-CL, ATR-FTIR and Micro-Raman) of selected specific mortar portions, such as binder-rich or lump samples (mechanical separation), enable the characterization of the calcite origin (differentiation between anthropogenic and geogenic calcite) with the perspective of reusing the samples for following analyses and dating.

The acidification line to extract CO₂ was coupled to the so-called Lilliput graphitization line, for dealing with small carbonate samples (2.5 mg lump and 5.0 mg bulk).

Our procedure has been successfully applied to single lumps collected from Florentine natural hydraulic mortars to date Trebbio Castle construction phases.

The new proposed multi-analytical procedure allowed us to discard most of the samples, identifying problems that could affect their correct dating (step II, III). Consequently, the preparation and the following AMS measurements (step IV) focused on just those micro-samples that had been found suitable as the result of characterization in step III, exploiting the same material. The results obtained from the comparison of the mortars with the historical-archaeological hypothesis provided relevant insights into the construction history of the building.

This paper aims at emphasizing that it is only through a well-structured analytical procedure that it is possible to select suitable samples and approach for the dating of traditional historical mortars.

Methods

Carbonation test

The phenolphthalein test (standardized by UNI EN 14630, 2007) is carried out using a 1% solution of phenolphthalein in ethyl alcohol. Applied to the surface of the freshly cut sample.

Optical microscope

The Axioscope A.1 Zeiss transmitted light polarizing optical microscope, connected to a digital video camera, allowed for the acquisition of sample images in thin sections, which were processed using AxioVision software. The acquired images were further analyzed to obtain information on the morphological and morphometric characteristics of the samples using the ImageJ program.

X-ray powder diffraction (XRPD)

The mineralogical composition was analyzed using a Philips X'Pert PRO X-ray powder diffractometer (XRPD) with a Cu anticathode (wavelength $\lambda = 1.54 \text{ \AA}$). The instrument operated at a current intensity of 30 mA and a voltage of 40 kV. The 2θ range explored was between 3 and 70° with a step size of 0.02° and a total time per pattern of 16 min 27 s. XRPD analyses were conducted on both powder bulk samples and specific lumps.

Scanning electron microscopy with energy-dispersive X-ray spectroscopy (SEM–EDS)

The ZEISS EVO MA 15 SEM–EDS with a tungsten filament and an energy-dispersive X-ray spectroscopy (EDS) analytical system, Oxford Ultimex 40 (with a resolution of 127 eV @5.9 keV and an area of 40 mm²), was utilized for semi-quantitative microchemical and morphological analyses. These analyses were conducted on thin sections (prepared after carbon-metallized pretreatment) taken from both the binder and lumps areas, as well as from powder samples. The operational settings were as follows: an acceleration potential of 15 kV, a beam current of 500 pA, a working distance of 9–8.5 mm, a live time of 20 s to achieve an acquisition rate of at least 600,000 counts using Co standard, a process time of 4 for point analyses, and a pixel dwell time of 500 μ s for map acquisition with a resolution of 1024 \times 768 pixels. The microanalysis employed the Aztec 5.0 SP1 software, implementing the XPP matrix correction scheme. This process utilized purchased standard elements for calculations, enabling “standard-less” quantitative analysis. Constant analytical conditions, such as filament emission, were monitored through numerous analyses of a Co metallic standard.

Thermo-gravimetric analysis (TGA)

Thermogravimetric analyses (TGA) were carried out on historical mortar samples using a Perkin Elmer Pyris 6 system and Netzsch TG 209 F3 Tarsus. Fragments from each sample were mechanically broken down using a porcelain pestle, and the portion passing through a sieve with 63 μm openings (ISO R 565 Series) was selected as a binder-rich specimen. About 5 mg of the sample was used for TGA, and the analysis was conducted within the temperature range of 110–1000 $^{\circ}\text{C}$. The samples were dried using silica gel as a desiccant at room temperature for a minimum of one week. The TGA experiments were performed in open alumina crucibles, with a heating rate of 10 $^{\circ}\text{C min}^{-1}$, and a nitrogen gas flow of 30 mL min^{-1} .

Cathodoluminescence (OM-CL)

Optical microscope cathodoluminescence (OM-CL) analysis was conducted using the CL8100 MK5 model by Cambridge Image Technology Ltd., coupled with a Leica DM2700P polarization optical microscope. The microscope is equipped with a high-sensitivity 12 MP Leica Flexcam C1 camera and dedicated LAS X software, enabling the acquisition of digital images in various formats.

Fourier transform infrared spectroscopy (ATR-FTIR)

FTIR spectra were collected with a portable Bruker Optics ALPHA FT-IR Spectrometer equipped with SiC Global source and a DTGS detector. The powdered samples were analyzed using a Platinum ATR single reflection diamond module collecting 24 scans, in the 4000–400 cm^{-1} spectral range, with a resolution of 4 cm^{-1} . The spectra were processed using OPUS 7.2 software (Bruker Optics GmbH, Ettlingen, Germany) and Spectragryph 1.2.15. Instrument was used in the laboratory of ISPC-CNR (Institute of Heritage Science in Sesto Fiorentino), Italy.

Micro-Raman spectroscopy

A Renishaw InVia Raman spectrometer, characterized by high resolution, was utilized in combination with a Leica DMLM microscope. The experiments involved employing a 785 nm excitation line, a 50 \times long working distance objective (NA 0.5), a spectral resolution better than 1 cm^{-1} , and a theoretical laser spot diameter of 1.9 μm . The laser operated at a power of 80 mW, and each spectrum was acquired over a period of 5 s. Our focus was primarily on the low-to-medium region of the spectral range, specifically collecting data within the range of 100–1400 cm^{-1} .

Data availability

All data generated or analysed during this study are included in this published article [and its supplementary information files].

Received: 18 March 2024; Accepted: 21 August 2024

Published online: 28 August 2024

References

- Hajdas, I. *et al.* Radiocarbon dating. *Nat. Rev. Methods Primers* **1**(1), 62. <https://doi.org/10.1038/s43586-021-00058-7> (2021).
- Urbanová, P., Boaretto, E. & Artioli, G. The state-of-the-art of dating techniques applied to ancient mortars and binders: A review. *Radiocarbon* **62**(3), 503–525. <https://doi.org/10.1017/RDC.2020.43> (2020).
- Hendriks, L. *et al.* Selective dating of paint components: Radiocarbon dating of lead white pigment. *Radiocarbon* **61**(2), 473–493. <https://doi.org/10.1017/RDC.2018.101> (2019).
- Strunk, A., Olsen, J., Sanei, H., Rudra, A. & Larsen, N. K. Improving the reliability of bulk sediment radiocarbon dating. *Quat. Sci. Rev.* **242**, 106442. <https://doi.org/10.1016/j.quascirev.2020.106442> (2020).
- Calandra, S. *et al.* Radiocarbon dating of straw fragments in the plasters of ST. Philip Church in archaeological site hierapolis of Phrygia (denizli, Turkey). *Radiocarbon* **65**(2), 323–334. <https://doi.org/10.1017/RDC.2023.20> (2023).
- Vasco, G. *et al.* Mortar characterization and radiocarbon dating as support for the restoration work of the Abbey of Santa Maria di Cerrate (Lecce, South Italy). *Heritage* **5**(4), 4161–4173. <https://doi.org/10.3390/heritage5040215> (2022).
- Al-Bashaireh, K. Plaster and mortar radiocarbon dating of Nabatean and Islamic structures, South Jordan. *Archaeometry* **55**(2), 329–354. <https://doi.org/10.1111/j.1475-4754.2012.00677.x> (2013).
- Goedicke, C. Dating mortar by optically stimulated luminescence: A feasibility study. *Geochronometria* **38**(1), 42–49. <https://doi.org/10.2478/s13386-011-0002-0> (2011).
- Panzeri, L., Maspero, F., Galli, A., Sibilia, E. & Martini, M. Luminescence and radiocarbon dating of mortars at Milano-Bicocca laboratories. *Radiocarbon* **62**(3), 657–666. <https://doi.org/10.1017/RDC.2020.6> (2020).
- Urbanová, P. *et al.* The Late Antique suburban complex of Santa Giustina in Padua (North Italy): New datings and new interpretations of some architectural elements. *Hortus Artium Medieval.* **28**, 185–200. <https://doi.org/10.1484/J.HAM.5.134911> (2022).
- Folk, R. & Valastro, S. Successful technique for dating of lime mortar by carbon-14. *J. Field Archaeol.* **3**, 2 (1976).
- Van Strydonck, M., Dupas, M. & Dauchot-Dehon, M. Radiocarbon dating of old mortars. *PACT J.* **8**, 337–343 (1983).
- Heinemeier, J. *et al.* AMS 14C dating of lime mortar. *Nucl. Instrum. Methods Phys. B Beam Interact. Mater.* **123**(1–4), 487–495 (1997).
- Michalska, D., Czernik, J. & Goslar, T. Methodological aspects of mortars dating (Poznań, Poland, MODIS). *Radiocarbon* **59**(6), 1891–1906. <https://doi.org/10.1017/RDC.2017.128> (2017).
- Hajdas, I. *et al.* Preparation and dating of mortar samples—Mortar Dating Intercomparison Study (MODIS). *Radiocarbon* **59**(6), 1845–1858. <https://doi.org/10.1017/RDC.2017.112> (2017).
- Artioli, G. *et al.* Characterization and selection of mortar samples for radiocarbon dating in the framework of the MODIS2 intercomparison: Two compared procedures. *Radiocarbon* **1–14**, 2024. <https://doi.org/10.1017/RDC.2024.3> (2024).
- Lichtenberger, A., Lindroos, A., Raja, R. & Heinemeier, J. Radiocarbon analysis of mortar from Roman and Byzantine water management installations in the Northwest Quarter of Jerash, Jordan. *J. Archaeol. Sci. Rep.* **2**, 114–127. <https://doi.org/10.1016/j.jasrep.2015.01.001> (2015).
- Fedi, M. *et al.* Towards micro-samples radiocarbon dating at INFN-LABEC, Florence. *Nucl. Instrum. Methods Phys. Res. B Beams Interact. Mater. At.* **465**, 19–23. <https://doi.org/10.1016/j.nimb.2019.12.020> (2020).

19. Cantisani, E. *et al.* The mortars of Giotto's Bell Tower (Florence, Italy): Raw materials and technologies. *Constr. Build. Mater.* **267**, 120801. <https://doi.org/10.1016/j.conbuildmat.2020.120801> (2021).
20. Heinemeier, J., Ringbom, Å., Lindroos, A. & Sveinbjörnsdóttir, Á. E. Successful AMS 14C dating of non-hydraulic lime mortars from the medieval churches of the Åland Islands, Finland. *Radiocarbon* **52**(1), 171–204. <https://doi.org/10.1017/S0033822200045124> (2010).
21. Ringbom, Å., Lindroos, A., Heinemeier, J. & Sonck-Koota, P. 19 years of mortar dating: Learning from experience. *Radiocarbon* **56**(2), 619–635. <https://doi.org/10.2458/56.17469> (2014).
22. Gliozzo, E., Pizzo, A. & La Russa, M. F. Mortars, plasters and pigments—research questions and sampling criteria. *Archaeol. Anthropol. Sci.* **13**(11), 193. <https://doi.org/10.1007/s12520-021-01393-2> (2021).
23. Boaretto, E. Dating materials in good archaeological contexts: The next challenge for radiocarbon analysis. *Radiocarbon* **51**(1), 275–281. <https://doi.org/10.1017/S0033822200033804> (2009).
24. Pesce, G. L., Ball, R. J., Quarta, G. & Calcagnile, L. Identification, extraction, and preparation of reliable lime samples for 14C dating of plasters and mortars with the “pure lime lumps” technique. *Radiocarbon* **54**(3–4), 933–942. <https://doi.org/10.1017/S0033822200047573> (2012).
25. Dilaria, S. *et al.* Phasing the history of ancient buildings through PCA on Mortars' Mineralogical Profiles: The example of the Sarno Baths (Pompeii). *Archaeometry* **1**–17, 2020. <https://doi.org/10.1111/arc.m.12746> (2020).
26. Miriello, D. *et al.* Characterisation of archaeological mortars from Pompeii (Campania, Italy) and identification of construction phases by compositional data analysis. *J. Archaeol. Sci.* **37**(9), 2207–2223. <https://doi.org/10.1016/j.jas.2010.03.019> (2010).
27. Cantisani, E., Fratini, F. & Pecchioni, E. Optical and electronic microscope for minero-petrographic and microchemical studies of lime binders of ancient mortars. *Minerals* **12**(1), 41. <https://doi.org/10.3390/min12010041> (2021).
28. Artioli, G., Secco, M., & Addis, A. *The Vitruvian legacy: Mortars and binders before and after the Roman world. The Contribution of Mineralogy to Cultural Heritage*, Gilberto Artioli, Roberta Oberti. <https://doi.org/10.1180/EMU-notes.20.4> (2019).
29. Arizzi, A. & Cultrone, G. Mortars and plasters—how to characterise hydraulic mortars. *Archaeol. Anthropol. Sci.* **13**(9), 144. <https://doi.org/10.1007/s12520-021-01404-2> (2021).
30. Pesce, G. The need for a new approach to the radiocarbon dating of historic mortars. *Radiocarbon* **65**(5), 1017–1021. <https://doi.org/10.1017/RDC.2023.92> (2023).
31. Calandra, S., Salvatici, T., Centauro, I., Cantisani, E. & Garzonio, C. A. The mortars of florence riverbanks: Raw materials and technologies of lungarni historical masonry. *Appl. Sci.* **12**(10), 5200. <https://doi.org/10.3390/app12105200> (2022).
32. Miyata, S. Anion-exchange properties of hydrotalcite-like compounds. *Clays Clay Miner.* **31**, 305–311. <https://doi.org/10.1346/CCMN.1983.0310409> (1983).
33. Ponce-Antón, G., Ortega, L. A., Zuluaga, M. C., Alonso-Olazabal, A. & Solaun, J. L. Hydrotalcite and hydrocalumite in mortar binders from the medieval castle of portilla (Álava, north Spain): Accurate mineralogical control to achieve more reliable chronological ages. *Minerals* **8**(8), 326. <https://doi.org/10.3390/min8080326> (2018).
34. Sabbioni, C. *et al.* Atmospheric deterioration of ancient and modern hydraulic mortars. *Atmos. Environ.* **35**(3), 539–548. [https://doi.org/10.1016/S1352-2310\(00\)00310-1](https://doi.org/10.1016/S1352-2310(00)00310-1) (2001).
35. Boynton, R. S. *Chemistry and Technology of Lime and Limestone* 2nd edn. (Wiley, 1980).
36. Bakolas, A. *et al.* Thermoanalytical research on traditional mortars in Venice. *Thermochim. Acta* **269**, 817–828. [https://doi.org/10.1016/0040-6031\(95\)02574-X](https://doi.org/10.1016/0040-6031(95)02574-X) (1995).
37. Moropoulou, A., Bakolas, A. & Bisbikou, K. Characterization of ancient, Byzantine and later historic mortars by thermal and X-ray diffraction techniques. *Thermochim. Acta* **269**, 779–795. [https://doi.org/10.1016/0040-6031\(95\)02571-5](https://doi.org/10.1016/0040-6031(95)02571-5) (1995).
38. Riccardi, M. P., Lezzerini, M., Car, F., Franzini, M. & Messiga, B. Microtextural and microchemical studies of hydraulic ancient mortars: Two analytical approaches to understand pre-industrial technology processes. *J. Cult. Herit.* **8**, 350–360. <https://doi.org/10.1016/j.culher.2007.04.005> (2007).
39. Marshall, J. D. Cathodoluminescence of geological materials by DJ Marshall, Unwin Hyman, 1988. <https://doi.org/10.1002/gj.3350260409> (1991).
40. Ricci, G. *et al.* Integrated multi-analytical screening approach for reliable radiocarbon dating of ancient mortars. *Sci. Rep.* **12**(1), 3339. <https://doi.org/10.1038/s41598-022-07406-x> (2022).
41. Toffolo, M. B., Ricci, G., Chapoulie, R., Caneve, L. & Kaplan-Ashiri, I. Cathodoluminescence and laser-induced fluorescence of calcium carbonate: A review of screening methods for radiocarbon dating of ancient lime mortars. *Radiocarbon* **62**(3), 545–564. <https://doi.org/10.1017/RDC.2020.21> (2020).
42. Lindroos, A., Heinemeier, J., Ringbom, Å., Braskén, M. & Sveinbjörnsdóttir, Á. Mortar dating using AMS 14C and sequential dissolution: Examples from medieval, non-hydraulic lime mortars from the Åland Islands, SW Finland. *Radiocarbon* **49**(1), 47–67. <https://doi.org/10.1017/S0033822200041898> (2007).
43. Murakami, T., Hodgins, G. & Simon, A. W. Characterization of lime carbonates in plasters from Teotihuacan, Mexico: Preliminary results of cathodoluminescence and carbon isotope analyses. *J. Archaeol. Sci.* **40**(2), 960–970. <https://doi.org/10.1016/j.jas.2012.08.045> (2013).
44. Chu, V., Regev, L., Weiner, S. & Boaretto, E. Differentiating between anthropogenic calcite in plaster, ash and natural calcite using infrared spectroscopy: Implications in archaeology. *J. Archaeol. Sci.* **35**(4), 905–911. <https://doi.org/10.1016/j.jas.2007.06.024> (2008).
45. Regev, L., Poduska, K. M., Addadi, L., Weiner, S. & Boaretto, E. Distinguishing between calcites formed by different mechanisms using infrared 236 spectrometry: Archaeological applications. *J. Archaeol. Sci.* **37**(12), 3022–3029. <https://doi.org/10.1016/j.jas.2010.06.027> (2010).
46. Toffolo, M. B., Regev, L., Dubernet, S., Lefrais, Y. & Boaretto, E. FTIR-based crystallinity assessment of aragonite–calcite mixtures in archaeological lime binders altered by diagenesis. *Minerals* **9**(2), 121. <https://doi.org/10.3390/min9020121> (2019).
47. Calandra, S. *et al.* Evaluation of ATR-FTIR spectroscopy for distinguishing anthropogenic and geogenic calcite. *J. Phys. Conf. Ser.* **2204**(1), 012048. <https://doi.org/10.1088/1742-6596/2204/1/012048> (2022).
48. Surovell, T. A. & Stiner, M. C. Standardizing infrared measures of bone mineral crystallinity: An experimental approach. *J. Archaeol. Sci.* **28**(6), 633–642. <https://doi.org/10.1006/jasc.2000.0633> (2001).
49. Seymour, L. M., Keenan-Jones, D., Zanzi, G. L., Weaver, J. C. & Masic, A. Reactive ceramic aggregates in mortars from ancient water infrastructure serving Rome and Pompeii. *Cell Rep. Phys. Sci.* **3**, 9. <https://doi.org/10.1016/j.xcrp.2022.101024> (2022).
50. Seymour, L. M. *et al.* Hot mixing: Mechanistic insights into the durability of ancient Roman concrete. *Sci. Adv.* **9**(1), eadd1602. <https://doi.org/10.1126/sciadv.add1602> (2023).
51. Bischoff, W. D., Sharma, S. K. & MacKenzie, F. T. Carbonate ion disorder in synthetic and biogenic magnesian calcites: A Raman spectral study. *Am. Min.* **70**(5–6), 581–589 (1985).
52. Borromeo, L. *et al.* Raman spectroscopy as a tool for magnesium estimation in Mg-calcite. *J. Raman Spectrosc.* **48**(7), 983–992. <https://doi.org/10.1002/jrs.5156> (2017).
53. Zolotoyabko, E. *et al.* Differences between bond lengths in biogenic and geological calcite. *Cryst. Growth Des.* **10**(3), 1207–1214. <https://doi.org/10.1021/cg901195t> (2010).
54. Wehrmeister, U. *et al.* Amorphous, nanocrystalline and crystalline calcium carbonates in biological materials. *J. Raman Spectrosc.* **42**(5), 926–935. <https://doi.org/10.1002/jrs.2835> (2011).
55. Calandra, S., Conti, C., Centauro, I. & Cantisani, E. Non-destructive distinction between geogenic and anthropogenic calcite by Raman spectroscopy combined with machine learning workflow. *Analyst* <https://doi.org/10.1039/D3AN00441D> (2023).

56. Toffolo, M. B. *et al.* Crystallinity assessment of anthropogenic calcites using Raman micro-spectroscopy. *Sci. Rep.* **13**, 12971. <https://doi.org/10.1038/s41598-023-39842-8> (2023).
57. Fedi, M. E., Cartocci, A., Manetti, M., Taccetti, F. & Mandò, P. A. The 14C AMS facility at LABEC. *Florence. Nucl. Instrum. Methods Phys. Res. B Beam Interact. Mater. At.* **259**(1), 18–22. <https://doi.org/10.1016/j.nimb.2007.01.140> (2007).
58. Arrighetti, A. *Materials and building techniques in Mugello from the Late Middle Ages to the Early Modern Age: Materiali e tecniche costruttive del Mugello tra basso Medioevo e prima Età Moderna.* <https://doi.org/10.3989/arq.arqt.2016.001> (2017).
59. Brogiolo G. P. & Cagnana A. *Archeologia dell'architettura. Metodi e interpretazioni* (ed. All'insegna del Giglio) (2012).
60. Vasari, G. *Le vite de' più eccellenti architetti, pittori, et scultori italiani, da Cimabue insino a' tempi nostri. Nell'edizione per i tipi di Lorenzo Torrentino, Firenze 1550* (ed. Einaudi) (2015).
61. Fratini, F., Cantisani, E., Pecchioni, E., Pandeli, E. & Vettori, S. Pietra Alberese: Building material and stone for lime in the Florentine Territory (Tuscany, Italy). *Heritage* **3**(4), 1520–1538. <https://doi.org/10.3390/heritage3040084> (2020).
62. Pavia, S. Repair mortars for masonry bridges. In *Bridge and Infrastructure in Ireland, Proc. 3rd Symp, Dublin* (2006).
63. Pecchioni, E., Fratini, F. & Cantisani, E. *Atlas of the Ancient Mortars in Thin Section under Optical Microscop* 2nd edn. (Nardini, 2020).
64. Ellerbrock, R., Stein, M. & Schaller, J. Comparing amorphous silica, short-range-ordered silicates and silicic acid species by FTIR. *Sci. Rep.* **12**, 11708. <https://doi.org/10.1038/s41598-022-15882-4> (2022).

Acknowledgements

The authors would like to thank Arch. Lucrezia Cuniglio, for the support and the collaboration for the collection of samples. Additionally, appreciation is extended to Laura Chiarantini and Tiziano Catalani for their technical assistance in the SEM-EDS analysis, as well as to Silvia Danise and Elena Pecchioni for facilitating access to OM-CL instrumentation.

Author contributions

S.C., E.C., C.C., M.F. designed the research; E.C., M.F., C.A.G. supervised the research project; F.F., A.A., T.S. archaeological and architectural research; F.F. E.C. collected and prepared the samples; S.C., E.C. OM, XRPD, SEM-EDS characterizations; S.C., C.C. Micro-Raman measurements; S.C., B.S. FTIR measurements; S.B., L.L., S.C. micro-sample preparation; M.F., S.B., L.L. AMS measurements and data analysis; S.C., E.C., M.F., S.B., L.L., A.A., F.F. archaeometric interpretation of results. All authors collaborated to the writing of the manuscript.

Competing interests

The authors declare no competing interests.

Additional information

Supplementary Information The online version contains supplementary material available at <https://doi.org/10.1038/s41598-024-70763-2>.

Correspondence and requests for materials should be addressed to S.C.

Reprints and permissions information is available at www.nature.com/reprints.

Publisher's note Springer Nature remains neutral with regard to jurisdictional claims in published maps and institutional affiliations.

Open Access This article is licensed under a Creative Commons Attribution-NonCommercial-NoDerivatives 4.0 International License, which permits any non-commercial use, sharing, distribution and reproduction in any medium or format, as long as you give appropriate credit to the original author(s) and the source, provide a link to the Creative Commons licence, and indicate if you modified the licensed material. You do not have permission under this licence to share adapted material derived from this article or parts of it. The images or other third party material in this article are included in the article's Creative Commons licence, unless indicated otherwise in a credit line to the material. If material is not included in the article's Creative Commons licence and your intended use is not permitted by statutory regulation or exceeds the permitted use, you will need to obtain permission directly from the copyright holder. To view a copy of this licence, visit <http://creativecommons.org/licenses/by-nc-nd/4.0/>.

© The Author(s) 2024